6B.4 A MIXED-PHASE CLOUD PARAMETERIZATION FOR USE IN A MESOSCALE NON-HYDROSTATIC MODEL: SIMULATIONS OF A SQUALL LINE AND OF OROGRAPHIC PRECIPITATION

Jean-Pierre PINTY*[1] and Patrick JABOUILLE[2]

[1]Laboratoire d'Aérologie, Toulouse, France
[2]Météo-France, Toulouse, France

1. INTRODUCTION

It is now widely accepted that accurate simulations of most precipitating events cannot be achieved while ignoring microphysical processes involving ice particles. However, due to many uncertainties in the mean properties of large classes of ice types and distributions, and also due to the poor knowledge of many empirical coefficients employed in the parameterization of specific processes, it seems wise to first consider simplified but robust schemes which give understandable results in various case studies (Mc Cumber et al., 1991). In the following, we present the main features of the standard mixed-phase scheme which is implemented in the non-hydrostatic "MésoNH" model. First we address some comments regarding the original aspects of the scheme and the choices made for some tunable parameters. Then the complete model is benchmarked on two very different 2D simulations but employing these same settings. The case of a tropical squall line of COPT81 (Chalon et al., 1988) is analysed in the light of previous studies made on such system (Caniaux et al., 1994). In the second case, a mid-latitude orographically forced precipitating event (Rauber 1992, hereafter R92) is reproduced with a realistic rain-snowfall transition pattern together with the maintenance of a supercooled cloud droplet region that was effectively detected during the SCPP85 field experiment.

2. A BRIEF REVIEW OF THE SCHEME

2.1 Generalities

In its essence, the scheme follows the approach of Lin et al. (1983) in that it is a three-class ice parameterization coupled to a Kessler's scheme for the warm processes. The scheme predicts the evolution of the mixing ratios of six water species: r_v (vapor), r_c and r_r (cloud droplets and rain drops) and r_i, r_s and r_g (pristine ice, snow/aggregates and frozen drops/graupels defined by an increasing degree of riming). The concentration c_i of the pristine ice crystals, here assumed to be plates, is diagnosed. The concentrations of the precipitating water drops and ice crystals are parameterized according to Caniaux et al. (1994), with the total number concentration $N = C\lambda^x$. λ is the slope parameter of the size distribution and $C - x$ empirical constants drawn from observations. The size distributions of the hydrometeors are assumed to follow a generalized γ-law: $g(D) = \alpha/\Gamma(\nu)\lambda^{\alpha\nu} D^{\alpha\nu-1} exp\big(-(\lambda D)^\alpha\big)$ in normalized form, which degenerates into the Marshall-Palmer law with $\alpha = \nu = 1$. Finally, simple power laws are taken for the mass-size ($m = aD^b$) and velocity-size ($v = cD^d$) relationships to perform useful analytical integrations. The complete characterization of each ice category and raindrops is summarize in the table below

Parameters	r_i	r_s	r_g	r_r
α, ν	3,3	1,1	1,1	1,1
a	0.82	0.02	196	524
b	2.5	1.9	2.8	3
c	800	5.1	124	842
d	1.00	0.27	0.66	0.8
C		5	$5\ 10^5$	10^7
x		1	-0.5	-1

Table 1: Set of parameters for each water specy

2.2 Overlook of the scheme

The pristine ice category is initiated by homogeneous nucleation (**HON**) when T$\leq -35^o$C, or more frequently by heterogeneous nucleation (**HEN**, here c_i is a simple function of the local supersaturation over ice). These crystals grow by water vapor deposition (**DEP**, see below) and by the Bergeron-Findeisen effect (**BER**). The snow phase is initiated by autoconversion (**AUT**) of the primary ice crystals; it grows by deposition (**DEP**) of water vapor, by aggregation (**AGG**) through small crystal collection and by the light riming produced by impaction of cloud droplets (**RIM**) and of raindrops

* *Corresponding author address*:
Jean-Pierre Pinty, Laboratoire d'Aérologie, OMP, 14 av. E. Belin, 31650, Toulouse, France;
e-mail <pinjp@aero.obs-mip.fr>.

(**ACC**). The graupels are formed as a consequence of the heavy riming of snow (**RIM** and **ACC**) or by rain freezing (**CFR**) when supercooled raindrops come in contact with pristine ice crystals. Distinction between light and heavy riming is made on the basis of a critical size of the snowflake (droplets) or by estimation of the mean density of the resulting particle (raindrops). According to the heat balance equation, graupel can grow more efficiently in the (**WET**) mode than in the (**DRY**) mode when riming is very intense (as for hailstone embryos). In the latter case, the excess of non-freezable liquid water at the surface of the graupels is shed (**SHD**) to form raindrops. When T$\geq 0^o$C, the pristine crystals are immediately transformed into cloud droplets (**MLT**) while each snowflake is converted progressively (**CVM**) into a graupel which melts (**MLT**) during its fall. The other processes are those described by the Kessler scheme: autoconversion of cloud droplets (**AUT**), accretion (**ACC**) and rain evaporation (**EVA**). The cloud droplets excepted, each condensed water species has a non-zero fallspeed. The sedimentation (**SED**) of the pristine ice crystals enables the slow erosion of cirrus sheets for long term integrations.

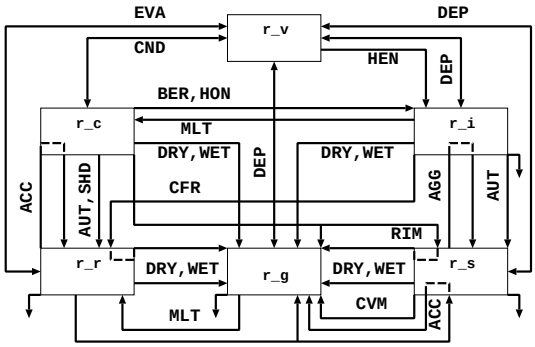

Diagram 1: Microphysical processes in the scheme

2.3 Some details of the scheme

One difficulty inherent to mixed-phase clouds is the possible coexistence of cloud droplets and small ice crystals, which necessitates a special treatment of the fast vapor exchanges (**DEP** and **CND**). As is usually done, the "floating" water vapor saturation pressure $r_{v_{c,i}}^{sat}$, is defined by a barycentric formula using the vapor saturation curves over water and ice and the mass amounts r_c and r_i, respectively. In the parameterization, the **DEP** and **CND** terms result in an implicit adjustment relative to $r_{v_{c,i}}^{sat}$, but with a new closure where any deficit/excess of r_v due to the adjustment, is compensated/absorbed by each phase in proportion to its actual amount. This is in contrast to other schemes where the closure is based upon an artificial linear function of temperature for 0 $\leq$T$\leq -40^o$C. The adjustment algorithm is non-iterative and 2^{nd} order accurate. Note that the **BER** effect is treated independently in an explicit way.

The other family of process that require careful treatment are the collection processes. When non-(r_c) or very little (r_i) precipitating categories are involved, the collection rates are computed analytically using the geometric sweep-out concept of the collection kernels. When both particules are precipitating, an analytical integration over the spectra is no longer possible and the use of pre-tabulated kernels have been preferred to approximate integrations. However in any case of ice-ice interaction, a major point of concern resides in the tuning of the sticking efficiencies which are still poorly understood functions of the temperature in most cases. After a series of experiments, the last set of coefficients retained by Ferrier et al. (1995) has been adopted in the scheme.

3. FIRST CASE STUDY: THE COPT81 TROPICAL SQUALL LINE

3.1 Numerical experiment

This case study is simulated with the same initial conditions and technique as in Caniaux et al. (1994). The collapse of an initial cold bubble triggers convection in narrow bands which leads to the development of an extended glaciated stratiform cloud mass downwind. We present averaged results on a 1/4 hour interval after 8 hours of simulation. A first comparison between the simulated and the observed (a 2D composite picture) radar reflectivity is shown in Fig. 1.

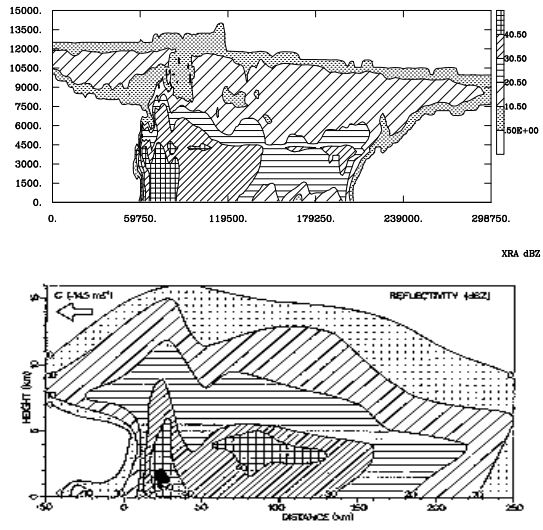

Figure 1: Modelled (top) and observed (bottom) reflectivity (from Chalon et al., 1985) with 10 dBZ contour interval.

One can see that the overall structure of the squall

line is reasonnably well reproduced by the model. Convective and stratiform regions, secondary maximum of reflectivity and forward overhang in the high levels can be observed on both plots. However, the simulated system suffers from an unsufficient vertical extent and the reflectivity is slightly underestimated in the stratiform region. Details of the microphysical fields are presented in Fig. 2.

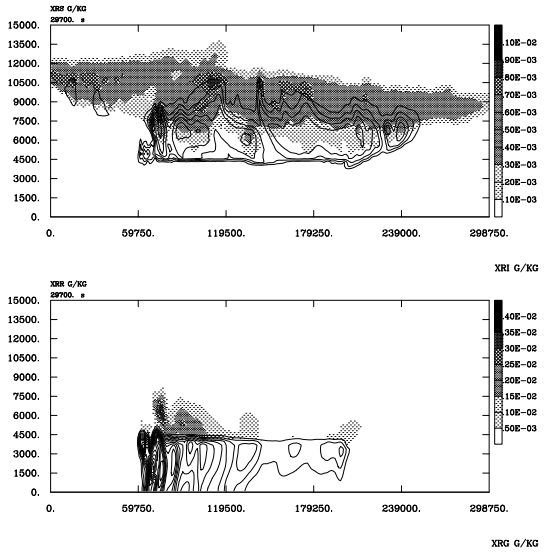

Figure 2: Top: r_i (grey scale) and r_s (solid lines). Bottom: r_g (grey scale) and r_r (solid lines) with contour interval of 0.5 g/kg for r_g and 0.1 g/Kg for $r_{i,s,r}$.

The simulation retrieves the classical vertical stratification with pristine ice in the highest levels ($r_i <$ 0.8 g/kg), then snow ($r_s < 1$ g/kg), and graupel just above the melting level. Maximum values of r_g (3.5 g/kg) and of r_r (1.5 g/kg) are found in the convective cells which produce the essential of the rainfall at a maximum rate of 50 mm/h. Evaporating rain below the glaciated stratiform region, which barely reaches the ground, helps to maintain the system.

4. SECOND CASE STUDY: THE SCPP85 OROGRAPHIC PRECIPITATIONS

4.1 Model set-up

This case study is extracted from the SCPP85 experiment. It has been documented by R92 as a typical, long lasting (36 hours between 12-13 February 1985) wintertime precipitating system across the ridge of the Sierra Nevada (California/Nevada) produced by moderately cold orographic clouds with a CTT$\geq -15^o$C. Previous simulations of this case were performed by Meyers and Cotton (1992, herafter MC92) in a 2D framework. MC92 found a great sensitivity of their results to the low level winds in the initial sounding, which lead to the formation of a blocked flow on the slope of the ridge. An equivalent set of simulations (300×55 points with $\Delta x = 1.5$km and $250 < \Delta z < 500$m) has been performed using MésoNH with very similar initial conditions and with a special start-up procedure. A 3 hour run has first been made with reversible warm microphysics (*i.e.*, a simple saturation adjustment) in order to build the flow dynamically with a bulk estimate of the latent heating. Because of this "cold" start-up phase, a 3D turbulence scheme is necessary to prevent unrealistic wave breaking over the coastal ridge upwind the Sierra. The model is then integrated for 2 additional hours, but now using the mixed-phase microphysical scheme with the restriction of no rain formation at T$< 0^o$C, to avoid an initial excessive raindrop freezing. During this stage, ice nucleation takes place and the growth by deposition of ice crystals leads to a rapid depletion of the initial cloud droplets r_c. As r_i grows, aggregation and riming occur, triggering the formation of snow r_s and graupel r_g. Finally, the full mixed-phase scheme is enabled and the simulation is run for at least 8 hours to test that the microphysical fields can effectively achieve a quasi stationnary state.

4.1 Results

The mean precipitation rates betwen 7-8 hours are plotted in Fig. 3. A snowfall peak of 2.4 mm/h occurs on the crest of the Sierra. A steady decrease of the precipitation rate is observed down to the Californian valley (Sacramento), while the decrease is sharper on the Nevada plateau (Tahoe) due to subsiding air aloft. The rain-snow transition takes place at mid-slope where precipitating rimed crystals (graupels) are also found (R92).

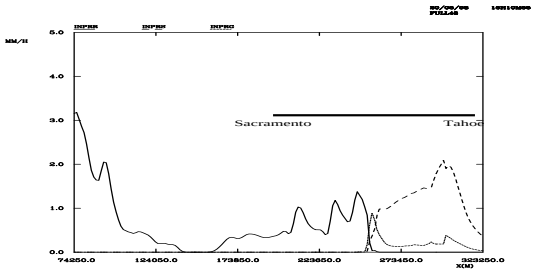

Figure 3: Precipitation rates: rain (solid line), snow (dashed line) and graupel (dotted line).

These model results are verified by the 35 hour precipitation map shown in Fig. 4. The observed precipitation patterns are close to the simulated ones but the observed maximum seems located slightly upwind of the crestline, although the quantitative agreement is reasonnable ("averaged" maximal value of 2.6 mm/h). So despite the highly simplified initial conditions (2D run with a single R/S)

and the difficulty in simulating the blocked flow, the model seems to successfully reproduce quantitative and persistent multiphase precipitation over the Sierra.

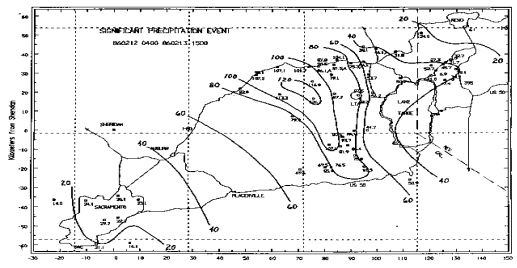

Figure 4: Precipitation map of the 35 hour event between Sacramento and Tahoe (by courtesy of A. Huggins of DRI)

The second point of interest in the simulation is related to the behaviour of the cloud and ice mixing ratio fields (Fig. 5). On the r_i plot, the trace of the isotherm 0^oC is delineated by the bottom of the cloud because the pristine ice crystals are immediately converted into cloud droplets when the temperature is positive. Looking now to the r_c plot above one can see that, surprisingly, the model is able to maintain a supercooled cloud droplet tongue ($r_c \sim 0.15$ g/kg) well within the glaciated cloud. This microphysical feature was observed during the SCPP field experiment as reported by R92, where heavy icing conditions were encountered by a research aircraft and also where radiometric detection of supercooled water could be made for similar events.

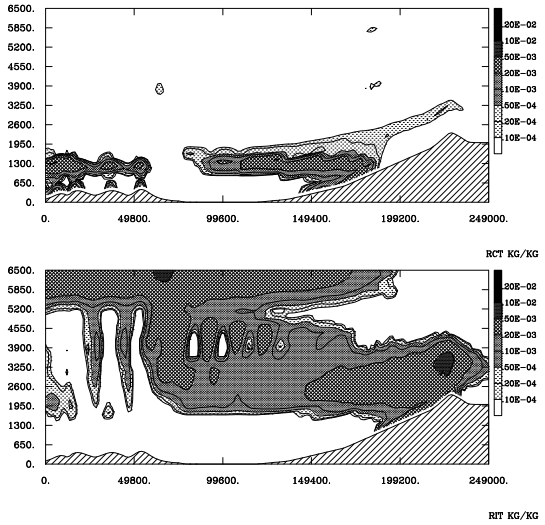

Figure 5: Simulated r_c (top) and r_i (botton) after 8 hours of integration of the full scheme (contours are in log scale).

The ability of the model to simulate a supercooled droplet region is very intringuing and must be analysed in detail. The existence of such situation requires a fine balance between the cloud droplet transport from the lower levels and the possible droplet sinks by riming or Bergeron-Findeisen effect. In fact, the supercooled droplets are colocated with the edge of the main snow zone production (not shown here) which is embedded in the glaciated area (Fig. 5). Note also that partial riming of the snowflakes in this area produces graupel which shows up in the precipitation rates of Fig. 3. Another point of discussion concerns the possible role of the Hallett-Mossop mecanism, not included in the present parameterization (c_i is simply diagnosed). By increasing c_i, this ice multiplication process could enhance the Bergeron-Findeisen conversion of the supercooled droplets and so limit their occurence. Thus although these preliminary results are very encouraging, they need to be confirmed by additional sensitivity experiments to determine the controling factors which favor the formation of supercooled droplets in such cases.

5. CONCLUSION

A bulk mixed-phase cloud model has been tested for two different situations. The case of a tropical squall line shows that the model is able to reproduce distinct microphysical states between the convective head, with sustained precipitation and the stratiform anvil where the evaporation of rain enables the maintenance of the system. In the second case, the simulation of an orographic system shows that the model can reproduce the pattern of multiphase precipitation while maintaining a region of supercooled cloud water in a realistic way.

6. REFERENCES

Caniaux, G., J.-L. Redelsperger, and J.-P. Lafore, 1994: A numerical study of the stratiform region of a fast-moving squall line. Part I: General description and water and heat budgets. *J. Atmos. Sci.*, **51**, 2046-2074.

Chalon, J-P., G. Jaubert, F. Roux, and J.-P. Lafore, 1988: The West African squall line observed on 23 june during COPT81. *J. Atmos. Sci.*, **45**, 2744-2763.

Ferrier, B. S., W.-K. Tao, and J. Simpson, 1995: A double-moment multiple-phase four-class bulk ice scheme. Part II: Simulations of convective storms in different large-scale environments and comparisons with other bulk parameterizations. *J. Atmos. Sci.*, **52**, 1001-1033.

Lin, Y.-L., R. D. Farley, and H. D. Orville, 1983: Bulk parameterization of the snow field in a cloud model. *J. Climate Appl. Meteor.*, **22**, 1065-1092.

McCumber, M., W.-K. Tao, J. Simpson, R. Penc, and S.-T. Soong, 1991: Comparaison of ice-phase microphysical parameterization schemes using numerical simulations of tropical convection. *J. Appl. Meteor.*, **30**, 985-1004.

Meyers, M. P., and W. R. Cotton, 1992: Evaluation of the potential for wintertime quantitative precipitation forecasting over mountainous terrain with an explicit cloud model. Part I: Two-dimensional sensitivity experiments. *J. Appl. Meteor.*, **31**, 26-50.

Rauber, R. M., 1992: Microphysical structure and evolution of a central Sierra Nevada orographic cloud system. *J. Appl. Meteor.*, **31**, 3-24.